AIP | Journal of Applied Physics

Decoupling small-scale roughness and long-range features on deep reactive ion etched silicon surfaces

Frank W. DelRio, Lawrence H. Friedman, Michael S. Gaither, William A. Osborn, and Robert F. Cook

Citation: J. Appl. Phys. **114**, 113506 (2013); doi: 10.1063/1.4821899
View online: http://dx.doi.org/10.1063/1.4821899
View Table of Contents: http://jap.aip.org/resource/1/JAPIAU/v114/i11
Published by the AIP Publishing LLC.

Additional information on J. Appl. Phys.

Journal Homepage: http://jap.aip.org/
Journal Information: http://jap.aip.org/about/about_the_journal
Top downloads: http://jap.aip.org/features/most_downloaded
Information for Authors: http://jap.aip.org/authors

ADVERTISEMENT

Instruments for advanced science

contact Hiden Analytical for further details
HIDEN ANALYTICAL
info@hideninc.com
www.HidenAnalytical.com
CLICK to view our product catalogue

JOURNAL OF APPLIED PHYSICS 114, 113506 (2013)

Decoupling small-scale roughness and long-range features on deep reactive ion etched silicon surfaces

Frank W. DelRio,[a] Lawrence H. Friedman, Michael S. Gaither, William A. Osborn, and Robert F. Cook
Materials Measurement Science Division, Material Measurement Laboratory, National Institute of Standards and Technology, Gaithersburg, Maryland 20899, USA

(Received 14 May 2013; accepted 5 September 2013; published online 19 September 2013)

A methodology to decouple irregular small-scale roughness and regular long-range features on deep reactive ion etched (DRIE) silicon surfaces is presented. Height-height correlations of three different DRIE silicon surfaces are evaluated via atomic force microscopy height data and fit to an analytic, five-parameter model based on a phenomenological scaling function for the small-scale roughness and a Bessel function for the long-range features. The resulting roughness parameters are constant for all three surfaces at small lateral length scales, indicating self-affine roughness inherent to the DRIE process, but dependent on the etch process at large lateral length scales, increasing by a factor of five as the controlled portion of the DRIE process decreased. The results from the analysis are also compared to fracture strengths from recently introduced "theta" test samples with the same etch features as an example of the potential of the analysis in providing an unbiased assessment of the processing-structure-property relationships for DRIE silicon surfaces.
[http://dx.doi.org/10.1063/1.4821899]

I. INTRODUCTION

The roughness of a surface is of great importance to a number of thin film technologies, as it directly controls many physical aspects of materials behavior (e.g., adhesion, friction, and strength) and, therefore, plays a role in the manufacturing yield and operational reliability of thin film devices. In some cases, surface roughness can be beneficial to device yield and reliability, for example, as a method to increase the average surface separation between micromachined surfaces, thus mitigating van der Waals and capillary meniscus adhesion in microelectromechanical systems (MEMS).[1–3] In other instances, surface roughness can be detrimental—critical flaws associated with roughness not only diminish the overall fracture strength of silicon (Si) MEMS, but, given a distribution of the flaw sizes, also bring about a wide distribution in the fracture strengths.[4–6] Independent of the nature of its influence, it is clear that surface roughness is critical to device performance and thus requires methods to quantify roughness metrics and correlate them to processing conditions and mechanical properties to achieve the materials science and engineering goal of producing processing-structure-property relations. Statistical height descriptors such as root mean square (rms) height and extreme value descriptors such as maximum peak-to-valley height are useful for describing height variations in the vertical direction, but contain no information about spatial variations in the lateral direction.[7] For instance, two sine waves with equal amplitudes, but different wavelengths, exhibit equivalent rms heights, but different spatial arrangements of surface heights. Therefore, both height descriptors and spatial functions are needed to adequately define surface roughness. Examples of common spatial functions include the height-height correlation function, the autocorrelation function, and the power spectral density function.[8,9] In particular, height-height correlation functions have been used to study the evolution of surface roughness during the growth[10,11] and etching[12,13] of Si, providing quantitative metrics related to the spatial and time scaling of surface roughness during different MEMS-relevant fabrication methods.

Despite the advances, however, there is still limited work on Si etching processes that induce both small-scale roughness and regular long-range features. Yang *et al.*[14] and later Gogolides *et al.*[15] studied etched Si surfaces with small-scale roughness and fairly regular three-dimensional mounds and found that the resulting height-height correlations exhibited undulations at length scales equal to the average mound separation. The latter group[16] later attempted to separate the two constituents simply by selecting a threshold surface height, which allowed the overall height distribution to be separated into its small (i.e., surface roughness) and large (i.e., regular mounds) components. In the work here, a new methodology to decouple small-scale roughness and regular long-range features is described. Deep reactive ion etched (DRIE) Si surfaces from the Bosch process[17] are examined, as this etch process is widely utilized in the MEMS industry to construct high aspect ratio devices with vertical sidewalls, albeit with characteristic etch steps called "scallops." Height-height correlations of three different DRIE Si surfaces are evaluated via atomic force microscopy (AFM) data and fit to an analytic, five-parameter model based on a phenomenological scaling function for the small-scale roughness and a Bessel function for the long-range scallops. To demonstrate a potential application, the resulting roughness parameters are compared to fracture strengths

[a]Author to whom correspondence should be addressed. Electronic mail: frank.delrio@nist.gov.

from recently introduced "theta" test samples[4–6] with the same etch features, allowing for an unbiased assessment of the processing-structure-property relationships for DRIE Si surfaces.

II. EXPERIMENTAL METHODS

Details about the fabrication process for the Si theta test samples can be found elsewhere.[6] Briefly, the test structures were formed on two different 100-mm (001) silicon-on-insulator (SOI) wafers; the resulting samples from each wafer are henceforth referred to as batches A and B. The device layers on both wafers were patterned with the same photolithographic mask, but etched using different Bosch DRIE processes. The two DRIE processes were designed to yield vertical sidewalls with distinct scallop dimensions; via changes to the passivation and etch times, the batch A samples were intended to exhibit smaller, more frequent, scallops than the batch B samples. The Si handle layers were then patterned and etched, and the SiO_2 layers were removed with a buffered-oxide etch to generate freestanding samples. Each test strip, consisting of 10 theta samples, was removed from the wafer with a scribe at notched regions at each end of the strip. The test strips were clamped into a fixture that was mounted into an AFM, such that the samples were upright and isolated from the surrounding clamp material. Intermittent-contact mode AFM was utilized to scan (5.0×5.0) μm^2 regions of the device layer sidewall surfaces at a line scan rate of 1 Hz and a resolution of (512×512) pixels, using AFM cantilevers with a nominal 40 N m^{-1} spring constant, 300 kHz resonance frequency, and 10 nm tip radius.

Figure 1 shows AFM images of the device layer sidewall surfaces for the batch A and batch B samples. As shown in Figs. 1(a) and 1(b), unintended variations in the batch A etch process led to two different surface structures: (a) *regular* etch features, or scallops, which were expected with the Bosch DRIE process, and (b) *irregular* etch features, or pits, which were likely formed when the SiO_2 layer between the Si device and handle layers fractured, leading to backside DRIE gases passing through the SiO_2 layer and re-etching the Si device layer.[5] In contrast, batch B samples exhibited only the intended surface structure; the scallop pitch for batch B samples was larger than that for batch A samples due to an increase in the passivation and etch step times and the ensuing decrease in the number of process loops needed to etch through the Si device layer, as shown in Fig. 1(c). The AFM surface height h data were used to calculate the angularly averaged height-height correlation function H according to[9]

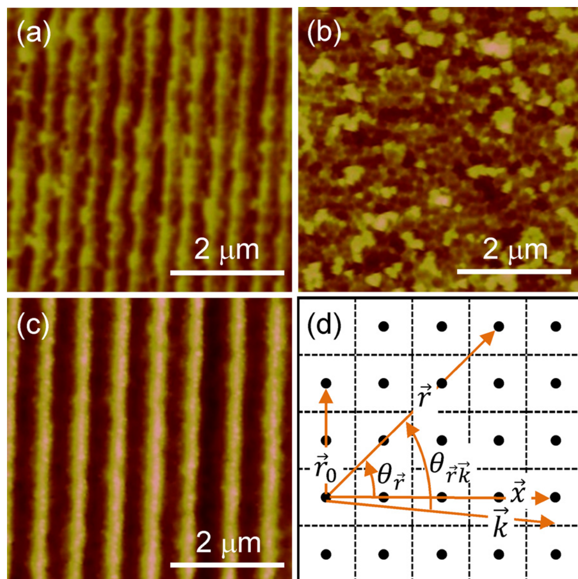

FIG. 1. (a)–(c) AFM images of the (a) small scallop, (b) pitting etch, and (c) large scallop surfaces. (d) Schematic depiction of a discrete Cartesian grid with pertinent angles and vectors.

$$H(r) = \langle [h(\vec{r} + \vec{r}_0) - h(\vec{r}_0)]^2 \rangle_{\vec{r}_0, \theta_{\vec{r}}}, \quad (1)$$

where $\langle \ \rangle$ signifies the statistical average of the square of the height difference between two points, with lateral separation distance r and heights $h(\vec{r} + \vec{r}_0)$ and $h(\vec{r}_0)$, over the choice of origin, $\vec{r}_0$, and the direction of $\vec{r}$, $\theta_{\vec{r}}$, as depicted in the schematic diagram in Fig. 1(d). H values were binned in annuli of small width ($\Delta r = 1$ pixel) to obtain continuous well-behaved angular averages of large sample size for H as a function of r. H for all three surfaces is presented in Fig. 2.

III. ANALYTICAL MODELS

For the pitting etch surface, H is well-described by the phenomenological scaling function[18]

$$H_r(r) = 2w^2[1 - \exp(-(r/\xi)^{2\alpha})], \quad (2)$$

where w is the rms roughness, ξ is the lateral correlation distance, and α is the roughness, or Hurst, exponent. For small lateral separations, $(r/\xi) \ll 1$, $H_r(r)$ approaches the asymptotic power-law scaling limit for a self-affine rough surface, $H_r(r) \sim (r/\xi)^{2\alpha}$, and for large separations, $(r/\xi) \gg 1$, $H_r(r)$ approaches the asymptotic invariant limit for a surface simply described by a rms roughness in which information about lateral height correlation scaling is absent, $H_r \sim 2w^2$. Note that $H_r(r)$ in Eq. (2) is a function of the scalar r and is thus an isotropic descriptor of roughness. Equation (2) provides a good fit to the pitting etch data in Fig. 2, consistent with the idea that the unconstrained backside DRIE gases distributed uniformly over the Si device layer leading to laterally isotropic etching, similar to that observed for ion-bombarded etch surfaces.[12,13]

Conversely, the H data for the batches A and B scallop surfaces, henceforth referred to as the small and large scallop surfaces, are not well-described by Eq. (2), most notably because the H values do not approach a single value, $2w^2$, at large r, and also because the values do not approach a single power law at small r. In particular, there are regular undulations in the data at large r, the first four of which are labeled (r_1 to r_4) in the inset of Fig. 2. The undulations at large r are indicative of long-range height correlations. Previous studies have observed similar undulations for Si surfaces with fairly regular three-dimensional mounds and linked the positions of the undulations to the average separation between nearby

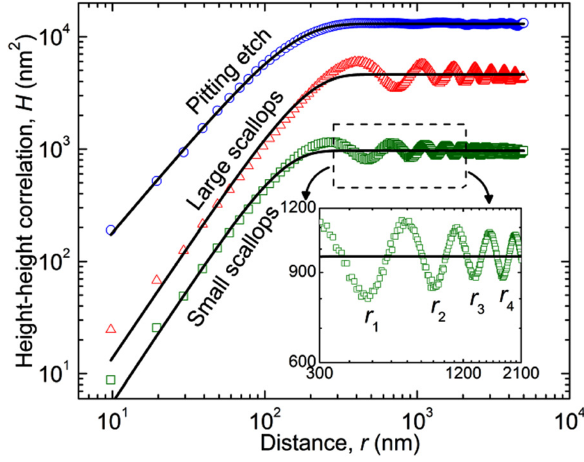

FIG. 2. Height-height correlation H as a function of lateral distance r for the small scallop, pitting etch, and large scallop surfaces. For the pitting etch, H is well-described by Eq. (2) over all r, as shown by the solid curve. Conversely, H for the scallop surfaces is not well-described by Eq. (2), particularly at large r, due to regular undulations in the data.

mounds.[14,15] The undulations for the mound surfaces quickly decayed to a steady-state H value, most likely because the long-range correlations diminished as r increased. In contrast, the undulations for the scallop surfaces in Fig. 2 extend out to the largest r values measured, indicating that the scallop pitch is consistent over the Si device layer. In both instances, however, it is clear that the overall H data are a combination of the H data from the underlying small-scale roughness and the regular long-range features, both of which are evident in Fig. 1. Hence, a clear determination of the former is only possible after the latter have been taken into account by decoupling the combined effects on the measured H behavior. The extracted values for α, ξ, and w from Eq. (2) for the best fits in Fig. 2 are given in Table I (in parentheses for the unmodified small and large scallop surface data).

The decoupling process involved two steps: (1) determine H for the scallops alone and then (2) add H for the scallops to H for the underlying roughness (Eq. (2)), such that the overall H can be fit to the experimental data. With regards to step 1, the simplest method to ascertain H for the scallops was to represent them as an extruded sine wave, such that the surface heights parallel to the scallops were constant and the surface heights perpendicular to the scallops were a function of $\vec{r}$ as given by $h_s(\vec{r}) = A\sin[\vec{k}\cdot\vec{r}]$, where A is the amplitude and $\vec{k}$ is the wavevector, Fig. 1(d). The magnitude of $\vec{k}$ is related to the scallop pitch or wavelength λ by means of $|\vec{k}| = 2\pi/\lambda$, and the direction of $\vec{k}$ is perpendicular to the scallop ridge lines (although we shall see that specification of the direction of $\vec{k}$ will not be required). H for the extruded sine was then found analytically by substituting $h_s(\vec{r})$ into Eq. (1), which results in

$$H_s(\vec{r}) = \langle \{A\sin[\vec{k}\cdot(\vec{r}+\vec{r}_0)] - A\sin[\vec{k}\cdot\vec{r}_0]\}^2\rangle_{\vec{r}_0,\theta_{\vec{r}}}. \quad (3)$$

After expanding the terms in the angular brackets and using trigonometric identities, Eq. (3) yields

$$H_s(\vec{r}) = \left\langle A^2\left\{1 - \frac{1}{2}\cos[2\vec{k}\cdot(\vec{r}+\vec{r}_0)] - \frac{1}{2}\cos[2\vec{k}\cdot\vec{r}_0] + \cos[\vec{k}\cdot(\vec{r}+2\vec{r}_0)] - \cos[\vec{k}\cdot\vec{r}]\right\}\right\rangle_{\vec{r}_0,\theta_{\vec{r}}}. \quad (4)$$

The average over $\vec{r}_0$ is performed first. The first, second, and third cosine terms oscillate with $\vec{r}_0$ and hence average to zero, while the constant A^2 and the fourth cosine term $A^2\cos[\vec{k}\cdot\vec{r}]$ are invariant with $\vec{r}_0$ and thus remain the same on averaging. The average over $\theta_{\vec{r}}$ on the remaining two terms is performed next, which is evaluated via explicit integration as given by

$$H_s(r) = \frac{1}{2\pi}\int_0^{2\pi} A^2\{1-\cos[kr\cos\theta_{\vec{r}\vec{k}}]\}d\theta_{\vec{r}\vec{k}} = A^2[1-J_0(kr)], \quad (5)$$

where $\theta_{\vec{r}\vec{k}}$ is the angle between $\vec{r}$ and $\vec{k}$ as shown schematically in Fig. 1(d) and J_0 is the zeroth-order Bessel function of the first kind. The asymptotic limits of $H_s(r)$ in Eq. (5) are $H_s(r) = (kr)^2/2$ at small separations, $(kr) \ll 1$, and $H_s(r) = A^2[1-(2/\pi kr)^{1/2}\cos(kr-\pi/4)]$ at large separations, $(kr) \gg 1$. Equation (5) is the basis for a broader class of integral transforms known as Hankel transforms,[19] which are especially useful during isotropic and angularly averaged correlation analyses.

Note that $H_s(\vec{r})$ in Eq. (3) is a function of the vector $\vec{r}$ and accounts for the anisotropy of the scallops and the specification of the vector $\vec{k}$. This anisotropy is not neglected on performing the angular average leading to $H_s(r)$ of Eq. (5), which depends on the scalar r, but cannot be recovered uniquely from Eq. (5) once the average has been performed. If the regular long-range features had been assumed to be isotropic, the integrand of Eq. (5) would contain no dependence on the angle $\theta_{\vec{r}\vec{k}}$. A measure of the effectiveness of the assumed extruded sine wave form for the scallops and the angular averaging to obtain a scalar function for $H_s(r)$ is how well Eq. (5) describes the experimental data, particularly at

TABLE I. Fit parameters for the extruded sine (A, λ) and surface roughness (α, ξ, w). The extracted values for α, ξ, and w prior to the extruded sine decoupling process are given in parentheses for reference. Uncertainty values represent one standard deviation from analysis of at least four images.

	Pitting etch	Small scallops	Large scallops
A (nm)		23.2 ± 0.4	60.4 ± 1.0
λ (nm)		426.1 ± 2.7	663.2 ± 2.0
α	0.80 ± 0.02	0.81 ± 0.06 (1.02 ± 0.01)	0.77 ± 0.02 (1.01 ± 0.01)
ξ (nm)	137.7 ± 4.2	165.3 ± 26.0 (126.0 ± 2.9)	164.5 ± 16.2 (177.1 ± 2.3)
w (nm)	77.4 ± 3.7	14.5 ± 0.3 (21.9 ± 0.2)	21.7 ± 1.6 (48.0 ± 0.9)

large r where the effects of small-scale roughness are expected to be small.

H_s for various A and λ are shown in Fig. 3. As illustrated in the examples, H_s exhibits many of the same features as the experimental H in Fig. 2, namely, power-law behavior at small r and regular undulations of diminishing magnitude at large r. In detail, however, it is clear that the specifics regarding H_s are significantly dependent on the values for A and λ. For example, it was found that λ determines the undulation positions; as λ increased by a factor of two, r_1 also increased by a factor of two (from P to P′). The positions of the minima in H_s are related to the odd-numbered roots of the first-order Bessel function J_1, such that $r_1 = 1.117\lambda$, $r_2 = 2.121\lambda$, $r_3 = 3.122\lambda$, $r_4 = 4.123\lambda$, and so on.[20] Analogous minima are observed in Fig. 2. In contrast, it was observed that A determines the magnitude of H_s; as A increased by a factor of two, H_s increased by a factor of four (from Q to Q′), or more generally, $H_s \sim A^2$ per Eq. (5). Overall, many of the details detected in Fig. 2 can be modeled via the inclusion of Eq. (5).

With regards to step 2 above, it has been previously established that the *autocorrelation* of the sum of two completely uncorrelated functions is the sum of the autocorrelations of each function.[8] Similarly, it can be proven that the *height-height correlation* of the sum of uncorrelated functions is simply the sum of the height-height correlations separately. As a result, H for the underlying small-scale roughness, H_r in Eq. (2), can be added to H for the regular scallop features, H_s in Eq. (5), to arrive at an analytic, five-parameter model for the measured height-height correlations

$$H_t(r) = 2w^2[1 - \exp(-(r/\xi)^{2\alpha})] + A^2[1 - J_0(kr)]. \quad (6)$$

IV. RESULTS AND DISCUSSION

H for the small and large scallop surfaces is shown in Fig. 4 and fit to $H_t(r)$ of Eq. (6). In both instances, H is well-described over all r, as shown by the solid curves. The extracted values for A, λ, α, ξ, and w are given in Table I.

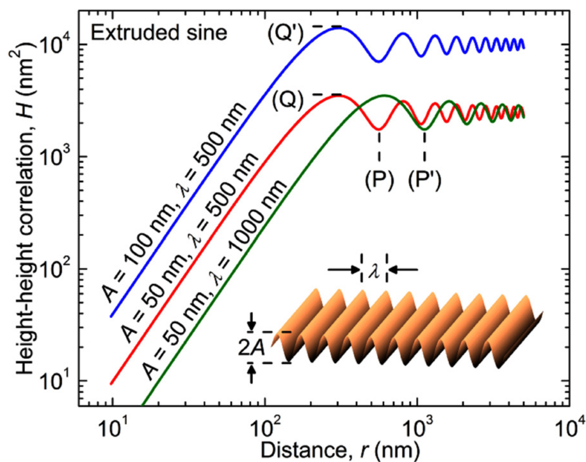

FIG. 3. Height-height correlation H as a function of lateral distance r for the extruded sine wave with different A and λ, as described by Eq. (5). From the examples, it was found that λ determines the undulation positions and A determines the magnitude of H_s.

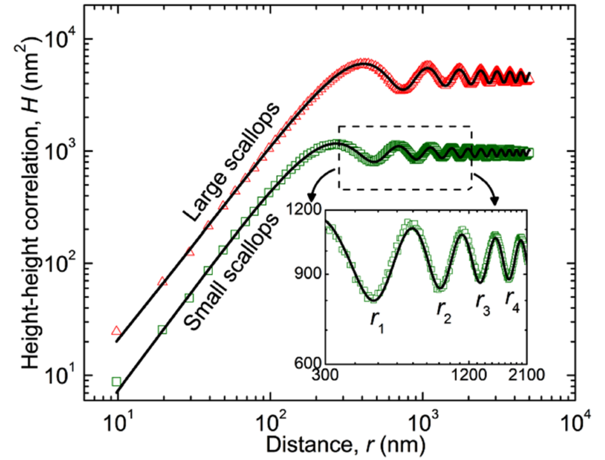

FIG. 4. Height-height correlation H as a function of lateral distance r for the small scallop and large scallop surfaces. In both instances, H is well-described by Eq. (6) over all r, as shown by the solid curves.

The results for λ are in good agreement with line scan measurements of the scallop pitch.[6] The height-height correlation approach to assessing λ is more robust than the line scan method, as it "averages" over an entire surface and is not sensitive to irregularities in the peaks and valleys or to detailed specification of the scallop orientation. The results for α also agree with previous experimental[15,21] and numerical[22,23] results on other plasma and reactive ion etched Si surfaces, where α ranged from 0.80 to 1.0. In addition, it is important to note that α was relatively *constant* at ≈ 0.80 for the three different surfaces (within experimental uncertainty). Hence, despite changes to the interscallop geometry, which represents the "controlled" or anisotropic part of the DRIE process, the scaling behavior for the intrascallop surface roughness, which is influenced by the "uncontrolled" or isotropic etch step, was unchanged. In fact, $\alpha \approx 0.80$ when the controlled portion of the etch was completely absent, as with the pitting etch surfaces, indicating that the outcome may be inherent to the DRIE process. In contrast, w *increased* from 14.5 nm to 21.7 nm to 77.4 nm as the surfaces changed from the small scallop to the large scallop to the pitting etch, respectively.

It is critical to note that quantitative assessment of the scaling of surface roughness features relies on separation of controlled and uncontrolled surface fabrication processes—in this case, separating the scallops superposed on the underlying roughness. As an example, fitting Eq. (2) to the experimental scalloped-surface height-height correlation data in Fig. 2 gave best fit power-law dependences in the small r region of "slope" $2\alpha \approx 2$ (values in parentheses in Table I). These dependences are very close to that of the small r asymptote of the height-height correlation function for the extruded sine wave, Eq. (5), implying that the scallops strongly affected the experimental height-height correlation over the full range of length scales, and not just at large r as might be expected. The analytical method used here to model the height-height correlation of the scalloped surfaces was extremely effective at describing the experimental observations, Fig. 4, suggesting that the choice of an extruded sine wave and angular averaging to arrive at a

scalar correlation function captured the main features of the anisotropic scallop geometry. Advantages of the method include easy addition of the scallop and small-scale roughness correlation functions as in Eq. (6), direct comparison with the annular bin-averaged experimental data from Eq. (1), and no requirement to specify wavevector directions in the images. Analyses that utilize vector height-height and other correlation functions for surface features[24,25] lose these advantages but could provide information regarding higher-order structure, both perpendicular and parallel to superposed long-range features, and information regarding potential anisotropy of underlying small-scale surface roughness. Such information will enable detailed refinements in nanoscale fabrication processes for surface-specific properties and applications.[1–6]

V. EXAMPLE APPLICATION

As mentioned previously, the etching processes used to create MEMS devices leave residual surface features such as surface roughness that can limit fracture strength, and consequently, device yield and reliability. As a result, it is necessary to determine the effects these etching processes have on MEMS device strength. To this end, micro-scale theta test specimens with the same etch features were tested using an instrumented indentation system and failure loads were converted to strengths via finite element analysis.[4–6] The resulting values were fit to a three-parameter Weibull distribution function

$$P_f = 1 - \exp\{-[(\sigma_f - \sigma_{th})/\sigma_\theta]^m\}, \quad (7)$$

where P_f is the cumulative failure probability, m is the Weibull modulus, σ_θ is the scaling strength, and σ_{th} is the threshold strength (the "characteristic strength," where $P_f = 0.632$, is $\sigma_c = \sigma_\theta + \sigma_{th}$). P_f was assigned to each strength value by $P_f = (i - 0.5)/N$, where i is the rank of the strength in an ascending-order ranked strength distribution and N is the number of samples. From the fits,[6] σ_c was found to be 2.22 GPa, 2.12 GPa, and 1.28 GPa for the small scallop, large scallop, and pitting etch surfaces, respectively. As shown in Table I, w was found to be 14.5 nm, 21.7 nm, and 77.4 nm and α was found to be relatively constant at ≈ 0.80 for the same surface sequence, suggesting an inverse correlation between σ_c and w and no connection between σ_c and α. Previous studies on the fracture strength of Si have alluded to the former trend,[26–30] but have largely ignored the latter relationship (or lack thereof), primarily due to their single-scale (large r) depictions of surface roughness. Both conclusions are only possible here because the analytic, five-parameter model presented above, Eq. (6), is based on a multi-scale (small and large r) representation of the roughness and scallops. In fact, fracture mechanics considerations suggest that σ_c should scale with w as $\sigma_c \sim (w + c_f)^{-1/2}$, where c_f is the length of a small, sharp crack located at the root of a rounded surface cavity of characteristic dimension w.[5] Taking $c_f = 5$ nm as common to all three DRIE surfaces, such scaling predicts strength ratios of 2.05:1.76:1 for the small scallop, large scallop, and pitting etch surfaces, which compares with 1.73:1.66:1 observed experimentally.[6] The agreement provides support for the ability of the model to provide quantitative characterization of surface properties.

It is important to note, however, that the aforementioned structure-property relationships are not based on an exhaustive study of the DRIE etch process and its effects on fracture strength, and therefore, the exact nature of the dependence requires additional experiments. For example, the two scalloped surfaces were formed via changes to both the passivation and etch DRIE steps, and as a result, exhibited changes to the small-scale roughness *and* long-range features. Consequently, the changes to σ_c cannot be entirely attributed to the changes in w, as both A and α are also varying (however, in a previous study,[6] it was hypothesized that σ_c should be independent of A and α because the loading direction is parallel, not perpendicular, to the scallops). Nevertheless, DRIE Si surfaces with similar small-scale roughness but different long-range features, and vice-versa, need to be evaluated with this method and tested with the theta test specimen, such that the effects of roughness and scallops on fracture strength can be decoupled. The decoupling process may be further enabled by additional studies on various pitting etch surfaces, as these surfaces are void of any long-range features.

VI. CONCLUSIONS

In conclusion, a new approach to decouple irregular small-scale roughness and regular long-range features on DRIE Si surfaces was presented. Three different sidewall surface structures were studied, two with the intended scallop features and one with an unintended pitting feature. Height-height correlations of the three different surfaces were evaluated via AFM height data and fit to an analytic, five-parameter model based on both the small-scale roughness and the long-range features. For all three surfaces, α was relatively constant at ≈ 0.80, suggesting the self-affine scaling behavior at small r was invariant regardless of the changes to the controlled portion of the DRIE process. In contrast, w differed with the etch, signifying that the vertical amplitude of fluctuations in the large r region was sensitive (varied by a factor of five) to the details of the process. The results from the analysis were finally compared to σ_c values from theta test samples with the same etch features. The comparison suggested an inverse correlation between σ_c and w and no correlation between σ_c and α. Future work on surfaces with different small-scale roughness and long-range features will elucidate the exact nature of the correlations, and in doing so, reach a materials science and engineering goal of forming a complete set of processing-structure-property relationships for DRIE Si surfaces.

ACKNOWLEDGMENTS

The authors thank Dr. Toh-Ming Lu at Rensselaer Polytechnic Institute and Dr. Yiping Zhao at the University of Georgia for useful discussions regarding height-height correlation properties. Certain commercial equipment, instruments, or materials are identified to specify the experimental procedure adequately. Such identification is not

intended to imply recommendation or endorsement by NIST, nor it is intended to imply that the materials or equipment identified are necessarily the best available for the purpose.

[1] F. W. DelRio, M. P. de Boer, J. A. Knapp, E. D. Reedy, P. J. Clews, and M. L. Dunn, Nature Mater. **4**, 629 (2005).

[2] F. W. DelRio, M. L. Dunn, L. M. Phinney, C. J. Bourdon, and M. P. de Boer, Appl. Phys. Lett. **90**, 163104 (2007).

[3] F. W. DelRio, M. L. Dunn, and M. P. de Boer, Scr. Mater. **59**, 916 (2008).

[4] M. S. Gaither, F. W. DelRio, R. S. Gates, E. R. Fuller, and R. F. Cook, Scr. Mater. **63**, 422 (2010).

[5] M. S. Gaither, F. W. DelRio, R. S. Gates, and R. F. Cook, J. Mater. Res. **26**, 2575 (2011).

[6] M. S. Gaither, R. S. Gates, R. Kirkpatrick, R. F. Cook, and F. W. DelRio, J. Microelectromech. Syst. **22**, 589 (2013).

[7] B. Bhushan, *Principles and Applications of Tribology* (Wiley, New York, 1999).

[8] J. S. Bendat and A. G. Piersol, *Engineering Applications of Correlation and Spectral Analysis* (Wiley, New York, 1993).

[9] H.-N. Yang, T.-M. Lu, and G.-C. Wang, *Diffraction from Rough Surfaces and Dynamic Growth Fronts* (World Scientific, Singapore, 1993).

[10] H.-N. Yang, G.-C. Wang, and T.-M. Lu, Phys. Rev. Lett. **73**, 2348 (1994).

[11] H.-N. Yang, Y.-P. Zhao, G.-C. Wang, and T.-M. Lu, Phys. Rev. Lett. **76**, 3774 (1996).

[12] H.-N. Yang, G.-C. Wang, and T.-M. Lu, Phys. Rev. B **50**, 7635 (1994).

[13] A. Chan and G.-C. Wang, Surf. Sci. **414**, 17 (1998).

[14] H.-N. Yang, Y.-P. Zhao, A. Chan, T.-M. Lu, and G.-C. Wang, Phys. Rev. B **56**, 4224 (1997).

[15] E. Gogolides, C. Boukouras, G. Kokkoris, O. Brani, A. Tserepi, and V. Constantoudis, Microelectron. Eng. **73–74**, 312 (2004).

[16] G. Boulousis, V. Constantoudis, G. Kokkoris, and E. Gogolides, Nanotechnology **19**, 255301 (2008).

[17] S. D. Senturia, *Microsystem Design* (Kluwer Academic Publishers, Boston, 2001).

[18] S. K. Sinha, E. B. Sirota, S. Garoff, and H. B. Stanley, Phys. Rev. B **38**, 2297 (1988).

[19] L. Debnath, *Integral Transforms and Their Applications* (CRC Press, Boca Raton, 1995).

[20] W. H. Beyer, *CRC Standard Mathematical Tables and Formulae* (CRC Press, Boca Raton, 1991).

[21] Y.-P. Zhao, J. T. Drotar, G.-C. Wang, and T.-M. Lu, Phys. Rev. Lett. **82**, 4882 (1999).

[22] J. T. Drotar, Y.-P. Zhao, T.-M. Lu, and G.-C. Wang, Phys. Rev. E **59**, 177 (1999).

[23] J. T. Drotar, Y.-P. Zhao, T.-M. Lu, and G.-C. Wang, Phys. Rev. B **61**, 3012 (2000).

[24] Y.-P. Zhao, G.-C. Wang, and T.-M. Lu, Phys. Rev. B **58**, 7300 (1998).

[25] T. Karabacak, Y.-P. Zhao, T. Liew, G.-C. Wang, and T.-M. Lu, J. Appl. Phys. **88**, 3361 (2000).

[26] F. Ericson and J.-A. Schweitz, J. Appl. Phys. **68**, 5840 (1990).

[27] T. Namazu, Y. Isono, and T. Tanaka, J. Microelectromech. Syst. **9**, 450 (2000).

[28] S. Sundararajan, B. Bhushan, T. Namazu, and Y. Isono, Ultramicroscopy **91**, 111 (2002).

[29] K.-S. Chen, A. A. Ayon, X. Zhang, and S. M. Spearing, J. Microelectromech. Syst. **11**, 264 (2002).

[30] D. C. Miller, B. L. Boyce, M. T. Dugger, T. E. Buchheit, and K. Gall, Sens. Actuators, A **138**, 130 (2007).